6th International Meeting
on
Wind Turbine Noise
Glasgow 20-23 April 2015

On the noise prediction of a serrated DU96 airfoil using the Lattice Boltzmann Method

W.C.P. van der Velden, A.H. van Zuijlen, A.T. de Jong & H. Bijl,
Aerodynamics Department, Faculty of Aerospace Engineering, Delft University of Technology, Kluyverweg 2, 2629 HT Delft, the Netherlands
Email: W.C.P.vanderVelden@TUDelft.nl

Summary

Computational fluid flow simulations around the open-source DU96 wind turbine airfoil are performed by means high Reynolds number Lattice Boltzmann solutions using the commercial solver Exa PowerFLOW 5.0b. The unsteady pressure distribution over the airfoil is used as an input for Ffowcs Williams-Hawkings analogy to predict the far field-noise. The broadband noise spectra's show clear non-compact dipole directivity and noise reduction is observed when serrations are applied.

1. Introduction

Far field noise can be considered as one of the main design drivers for on-shore wind turbines. Strict governmental regulations limit the power production of single turbines, especially during night when background noise is lower. A possible decrease of the sound pressure level by one single decibel would increase the annual energy production by 20% (Oerlemans and Fuglsang 2012). Therefore it is important to investigate possibilities to reduce noise of wind turbines, thereby increasing the power production and reducing the cost of energy.

Previous acoustic field measurements showed that the turbulent trailing edge noise of a wind turbine blade is currently one of the most dominant noise sources on a wind turbine and therefore understanding the physics associated with the generation and propagation is of main importance for the design of more silent wind turbines (Oerlemans, Sijtsma and Mendez Lopez 2007). This dominant type of noise is commonly known as airfoil self-noise and originates from unsteady flow over the turbine blade. Brooks, Pope, and Marcolini (1989) defined some fundamental self-noise mechanism such as the large-scale separation (deep stall) tip vortex, blunt trailing edge, laminar boundary layer and turbulent boundary layer noise. With turbulent flow, the acoustic effects depend largely on the length scale of the turbulent eddies (Blake 1986). For trailing edge noise this turbulent length scale is the boundary layer displacement thickness at the trailing edge, making the size of the eddies much smaller than the airfoil chord, thereby only effecting the local pressure fluctuations while keeping the global aerodynamic force similar. The sound of the turbulent eddies is scattered from the trailing edge towards the leading edge (i.e. in upstream direction). This typical trailing edge noise results in high-frequency edge noise.

To reduce trailing edge noise, Howe performed a numerical analysis of a flat plate, with the trailing edge modified by the presence of serrations possessing a saw tooth profile. Howe (1999) predicted that the intensity of radiation at the trailing edge could be reduced by such a modification, with the magnitude of the reduction depending on the length and spanwise spacing of the teeth, as well as the frequency of the radiation. It was determined that the dimensions of an individual serration should be at least of the order of the turbulent boundary layer thickness and that longer, more narrower teeth should yield a greater intensity reduction.

In addition, large-scale experiments on realistic wind turbine blades were performed by Oerlemans et al. (1999), and he found that adding serrations led to noise reductions of 2-3 dB. However, the effectiveness of serrations on the overall noise reduction is still not yet fully understood and might deal with, for example, a decrease in acoustical source terms, a shift of low frequency noise to higher frequencies or a change in sound diffraction due to the complex geometry. Hence, understanding the physics by which trailing edge serrations reduce airfoil self-noise is therefore of clear importance. If the physics were completely understood it could potentially lead to improvements in serration design, and possibly the development of improved, alternative techniques based on similar physical principles.

The current study illustrates the capabilities of a Lattice Boltzmann solver to solve the fluctuating turbulent boundary layer and pressure coherence being used for predicting the acoustic field around a complex and challenging geometry; a serrated wind turbine airfoil profile. The discrete Boltzmann equations are solved in combination with a collision model to simulate the flow of a Newtonian fluid. By simulating streaming and collision processes across a limited number of particles, the intrinsic particle interactions evince a microscale of viscous flow behavior applicable across the greater mass. Acoustic results are obtained by solving the non-homogeneous wave equation in time domain in combination with unsteady wall pressure sources.

2. Methodology

2.1. Governing flow equations

The results are obtained from numerical simulations of the Lattice Boltzmann Method (LBM) (Succi 2001). Instead of solving the traditional partial differential equations, known as the Navier-Stokes equations, the discrete Boltzmann equations are solved for simulating complex fluid flows. The LBM method starts from mesoscopic kinetic equations, i.e. the Boltzmann equation, to determine macroscopic fluid dynamics. The commercial software package Exa Powerflow 5.0b is used for this study, allowing a three-dimensional flow to be simulated in 19 directions (D3Q19). The kinetic equations are solved on a cartesian mesh, known as lattices, by explicit timestepping and collision modeling. The equation has the general form:

$$f_i(\mathbf{x} + \mathbf{c_i}\Delta t, t + \Delta t) - f_i(\mathbf{x}, t) = C_i(\mathbf{x}, t),$$

where f_i denotes the movement of the distribution of particles in the i-th direction, according to a finite set of discrete velocity vectors $\{c_i: i=0,\ldots,N\}$. $c_i\Delta t$ and Δt are space en time increments respectively. The collision term on the right hand side of the LBM equation adopts the simplest and also the most popular form known as the Bhatnagar-Cross-Krook (BGK) form (1954):

$$C_i(\mathbf{x}, t) = -\frac{\Delta t}{\tau}\left[f_i(\mathbf{x}, t) - f_i^{eq}(\mathbf{x}, t)\right].$$

In this collision term, τ denotes the relaxation time parameter, and f_i^{eq} is the local equilibrium distribution function, which depends on local fluid fluctuating properties. The basic fluid dynamic quantities, which do appear directly in the Navier-Stokes equations, such as fluid density ρ and velocity u, are obtained using moment summations over the velocity vectors:

$$\rho(\mathbf{x}, t) = \sum_i f_i(\mathbf{x}, t), \rho\mathbf{u}(\mathbf{x}, t) = \sum_i \mathbf{c_i} f_i(\mathbf{x}, t).$$

When considering the very low frequency and long wavelength limit, for a suitable choice of the set of discrete velocity vectors, the compressible Navier-Stokes equations can be recovered using the Chapman-Enskog expansion (Succi 2001). The resulting equation of state obeys the ideal gas law: $p = \rho R T$. The kinematic viscosity of the fluid is related to the relaxation time parameter, τ, according to Chen (1998):

$$\tau = \frac{\nu}{RT} + \frac{\Delta t}{2}.$$

Combining all previous equations will form the LBM scheme applied in this study. In addition, a viscosity model can be implemented through the relaxation time τ to locally adjust the numerical viscosity of the scheme (Chen 2003). The turbulence model that is incorporated into the Exa Powerflow 5.0b is used. The model consists of a two-equation k-ε Renormalization Group

(RNG) modified to incorporate a swirl-based correction that reduces the modeled turbulence in presence of large vortical structures. This approach is commonly known as a Very Large Eddy Simulation (VLES).

Fully resolving the near wall region is computationally too expensive for high-Reynolds number turbulent flow with the lattice concept of the LBM scheme. Therefore, a turbulent wall model is used to provide approximate boundary conditions. In the current study, the following wall-shear stress model based on the extension of the generalized law of the wall model is used (Chen 1998) (Crouse et al. 2007):

$$u^+ = f\left(\frac{y^+}{A}\right) = \frac{1}{\kappa}\ln\left(\frac{y^+}{A}\right) + B,$$

with

$$A = 1 + f\left(\frac{dp}{dx}\right).$$

and κ and B chosen in such a way, a turbulent boundary layer is modeled. This relation is iteratively solved to provide an estimated wall-shear stress for the wall boundary conditions in the LBM scheme. A slip algorithm (Chen 1998), a generalization of bounce-back and specular reflection process, is then used for the boundary process.

The LBM scheme inherently captures acoustic waves, since it models the compressible, transient Navier-Stokes equations, including ideal gas equation of state. The scheme is solved on a grid composed of cubic volumetric elements, the lattices. A variable resolution is allowed, where the grid size changes by a factor of two for adjacent resolution regions. Due to the explicit time-stepping characteristics of the LBM scheme, the time-step size is increased with cell size in factors of two as well. Larger cells will therefore not be evaluated each timestep of the smallest cell. This gives rise to the notion of timestep equivalent number of cells, which are the number of cells scaled to operation at the shortest timestep in addition to the total number of cells.

2.2. Determination of coherence

For determination of the coherence length, first the coherence function should be evaluated. The coherence function is the auto-power and cross-power density of the signals, where $\Phi(\omega,z_1,z_2)$ denotes the cross-power spectral density between two points along a given dimensional line $\Delta z=z_2-z_1$, with ω defined as the angular frequency:

$$\gamma^2(\omega,\Delta z) = \frac{|\Phi(\omega,z_1,z_2)|^2}{|\Phi(\omega,z_1,z_1)|\,|\Phi(\omega,z_2,z_2)|}.$$

This representation is valid for the case that the flow statistics are homogeneously distributed along the spatial dimension, stationary in time and for an infinite observation period. For a flat plate the first criterion is fulfilled when considering the spanwise direction, and with restriction to very short separations, also for the streamwise direction. The cross-power spectral densities are obtained using Welch's method in combination with a 50% overlap Hanning window.

By definition, the coherence length is related to the integral of coherence function over the spatial separation Δz and therefore reduces to a function of frequency only:

$$l_z(\omega) = \lim_{L\to\infty}\int_0^L \gamma(\omega,\Delta z)\,d\Delta z.$$

This relation can be used to obtain the coherence length. However, due to convergence issues with respect to simulation time, first observed by Christophe (2011) for his LES data with a finite observation period, the coherence does not approach zero for very large separations Δz and therefore, the integral might be unbounded. Instead, in this study a curve fitting approach based on an exponential function is applied (Palumbo 2012):

$$\gamma(\omega,\Delta z) = e^{-\frac{|\Delta z|}{l_z(\omega)}}.$$

The fit is performed for each discrete frequency and has shown to be a robust alternative to the integral solution.

2.3. Governing acoustic equations

Within the field of Computational Aero-Acoustics (CAA) a distinction is made between direct and hybrid methods. Direct CAA methods solve the full compressible flow equations for determining both the hydrodynamic and acoustic pressure fluctuations. The domain covers both the flow field and at least the source and near acoustic field. Due to the high computational cost originating from the large scale separation of hydrodynamic fluid and acoustic pressure fluctuations, a direct calculation is restricted to simple geometries and low and moderate Reynolds numbers. In a hybrid method the flow and acoustic field are calculated separately, so that the numerical method can be optimized for the physics to be solved.

To efficiently predict the noise propagation at arbitrary locations, an integrated parallelized post-processing module is available in PowerFLOW that uses the acoustic analogy solver based on the theory of the Ffowcs Williams-Hawkings (FW-H) equation (Brès, Pérot and Freed 2010). The solver is able to handle a motion of the noise generating solid geometry, either in a fluid at rest or in a uniform flow. The formulations are implemented in the time domain using a source-time dominant algorithm also referred to as an advanced time approach (Brès, Pérot and Freed 2010). The input to the FW-H solver is the time-dependent flow field on a surface mesh provided by the transient LBM simulations. This surface mesh is defined either as a solid surface corresponding to the physical body or as a permeable surface surrounding the solid body. For practical reasons, the present study uses the solid formulation, with pressure information recorded on the airfoil.

3. Model set-up

The model under consideration is the free transition DU96-W180 profile with a 600 mm chord at a Reynolds number of 1.5×10^6. 15% of the chord is modeled in spanwise direction to allow for a proper calculation of the spanwise coherence length. Three sub-models are considered, a clean model with no trailing edge add-on and two serrated trailing edge models of 5% and 15% of the chord respectively, with an width/length ratio of 0.5 under an angle of 0 degrees with respect to the chord whereas the total model (airfoil + serration) is positioned under an angle of 6 degrees.

The outer domain stretches 20 chord lengths in both directions, whereby the coarsest outer region holds an anechoic layer, to damp out the acoustical waves near the far field boundaries. At the inlet a velocity of 45 m/s is described, while the outlet is modeled by fixing the static pressure, while maintaining a free flow direction. The simulated Mach number is identical to the real Mach number, i.e. 0.13. The grid used in this study has 32×10^6 voxels, whereas 17×10^6 voxels are fine equivalent voxels, with 8 different refinement regions located around the airfoil. A detail of the domain is given in Fig. 1. The finest voxels, around the trailing edge are cubes of size 3.52×10^{-4} m in order to correctly determine the near wake. The boundary layer is modeled using the inbuilt wall model, with the closest cell located around $y^+ = 50$.

The Courant-Friedrichs-Lewy (CFL) stability number is set to unity by the solver inherently, to ensure stable conditions. In physical time, the simulations are run for 0.25 s which yields around 18 flow passes. Statistical data is recorded at a frequency of 26kHz.

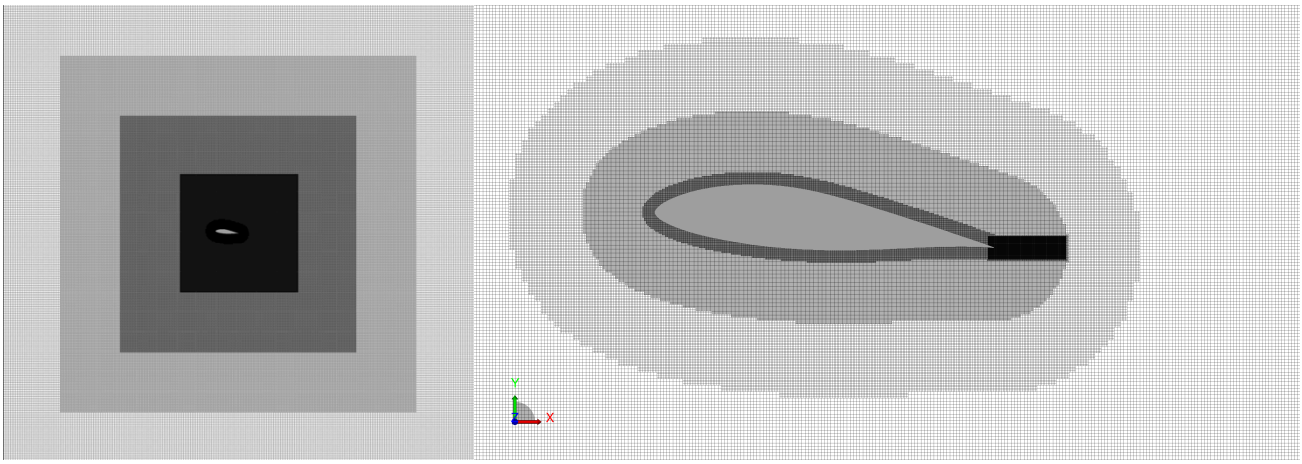

Figure 1: Refinement regions around DU96 profile

4. Fluid results

The flow results are first analysed by taking a closer look at the flow around the DU96 profile. An instantaneous velocity field plot around the airfoil is shown in Fig. 2 for the clean case. Strong acceleration occurs over the suction side due to the camber of the profile and flow incidence. Further towards the trailing edge, the flow becomes turbulent and a turbulent boundary layer develops and convects further over the trailing edge. The adverse pressure gradient thickens the boundary layer up to the trailing edge. On the pressure side, the boundary layer remains very thin and laminar. This observation is illustrated by looking at the boundary layer profile in Fig. 3, scaled by local outer variables. Clearly, the pressure side (PS) remains laminar (with a shape factor of 2.3) while at the suction side (SS), a fully turbulent boundary layer is observed (shape factor equals 1.4).

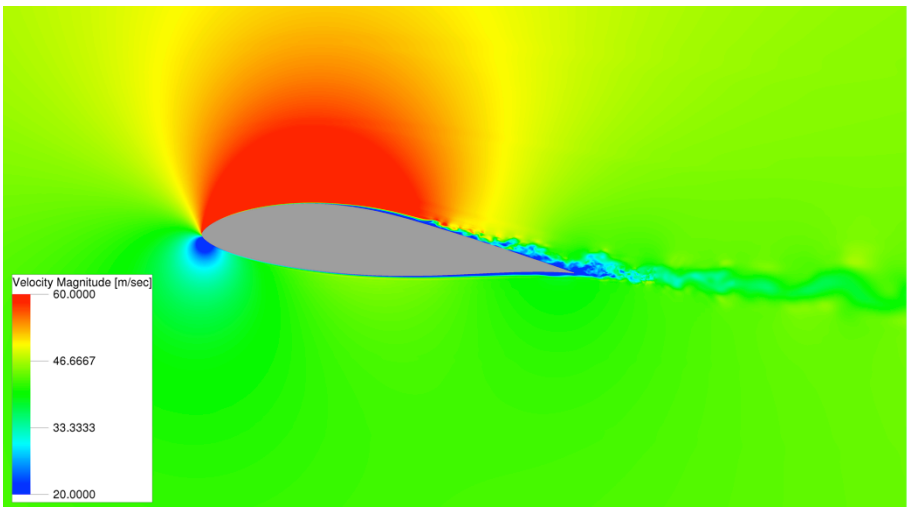

Figure 2: Instantaneous snap-shot of the velocity magnitude around the DU96 profile

The mean pressure distribution, shown in Fig. 4 for the clean profile case shows close resemblance at the complete pressure side for all three references. References include data extracted from XFOIL (Drela 1989), experimental data from NREL (Devenport et al. 2008) and numerical data from a LES simulation based on the Navier-Stokes equations (Wolf et al. 2012). The favourable pressure gradient near the leading edge for the suction side is under predicted in the current simulation, likely due to relatively large distance of the first cell. Transition is modelled slightly different as can been seen from the plot. Near the trailing edge however, where the size of the first lattice is reduced, a perfect match between the simulation and numerical references is found. A further study will include a mesh resolution study, to look at these discrepancies more closely.

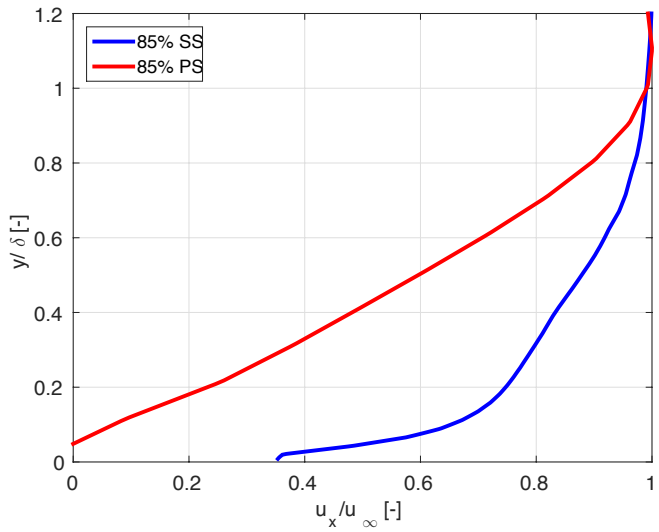

Figure 3: Outer scaled mean velocity

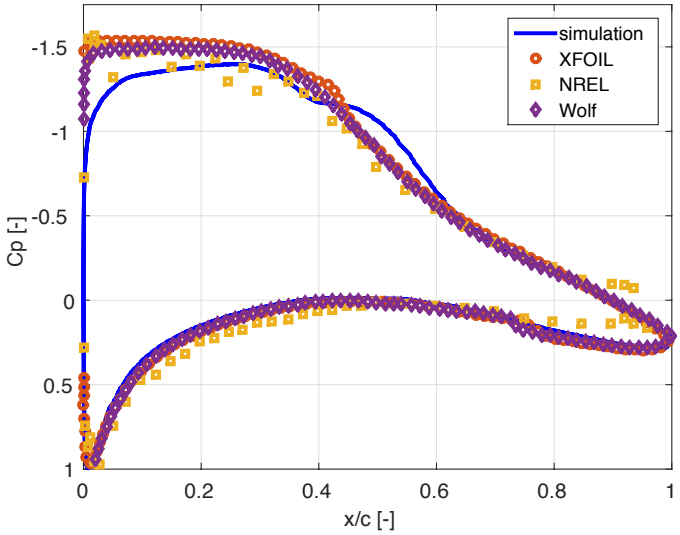

Figure 4: Mean pressure distribution

The bump around 0.4 x/c at the suction side of the profile in Fig. 4 suggests the transition from the laminar to the turbulent region. To closely look at the transition pattern, λ_2 iso-surfaces, which is the second largest eigenvalue of the sum of the square of the symmetrical and anti-symmetrical parts of the velocity gradient tensor, are plotted in Fig. 5. Initially, at the nose a fully stable laminar flow is present. Further downstream the suction side, Tolmien-Schlichting waves are formed, meaning that the critical Reynolds number has been exceeded and Kelvin Helmholtz instabilities are started. A very thin laminar recirculation bubble at 0.4 x/c triggers the transition to turbulence. The laminar separation attaches again at 0.45 x/c, and transition to the turbulent regime occurs. Within the turbulent boundary from Fig. 5, low-speed streaks (blue) and vortical structures (green to red) are qualitatively shown by means of hairpin packets, full hairpins, legs and cane vortices.

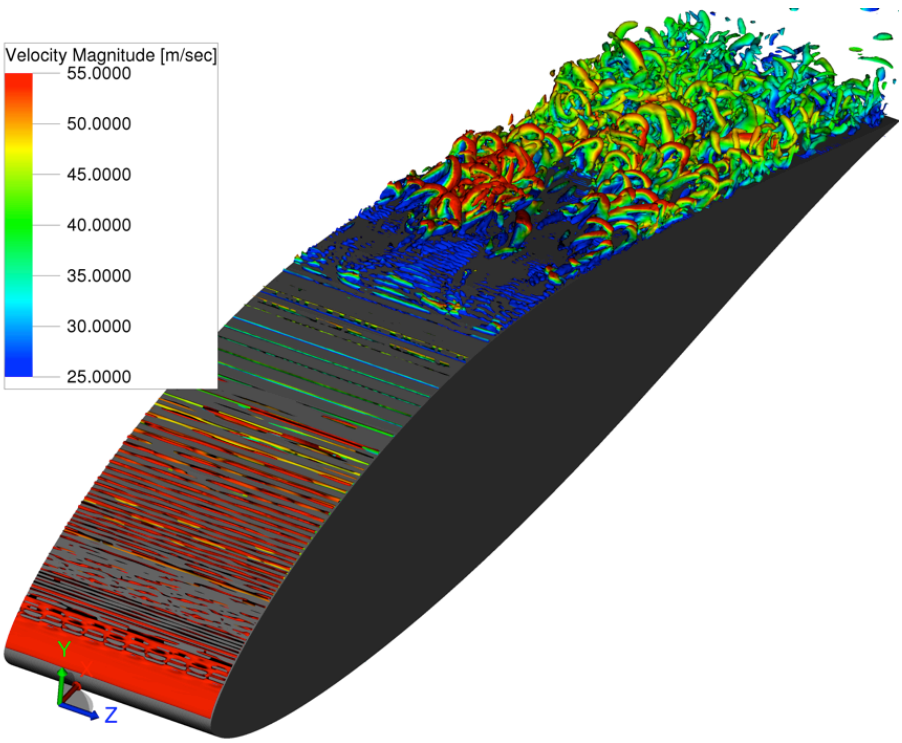

Figure 5: λ_2 (-750) iso-surface plot colored with velocity magnitude around the DU96 profile

Previous results were concerning the clean model only. When attaching the serrations, the flow and pressure changes in the close vicinity of the serration. To qualitatively illustrate some of the changes, λ_2 iso-surfaces near the trailing edge region are depicted in Fig. 6. For the clean profile, the laminar boundary layer on the pressure side generates small vortices at the bottom

of the wake because of the blunt trailing edge. They are destabilized due to mixture with the turbulent boundary layer from the suction side. In the serrated case, the flow is sucked through the teeth of the serrations from the pressure to the suction side. Over the serrations, close to the boundary, the turbulent structures are destructed and stretched out; no hairpins and hairpin legs are visible anymore whereas in the clean case, hairpin legs stay visible in the near wake. The serrated edges increase the thickness of the far wake, likely due to enhanced mixing.

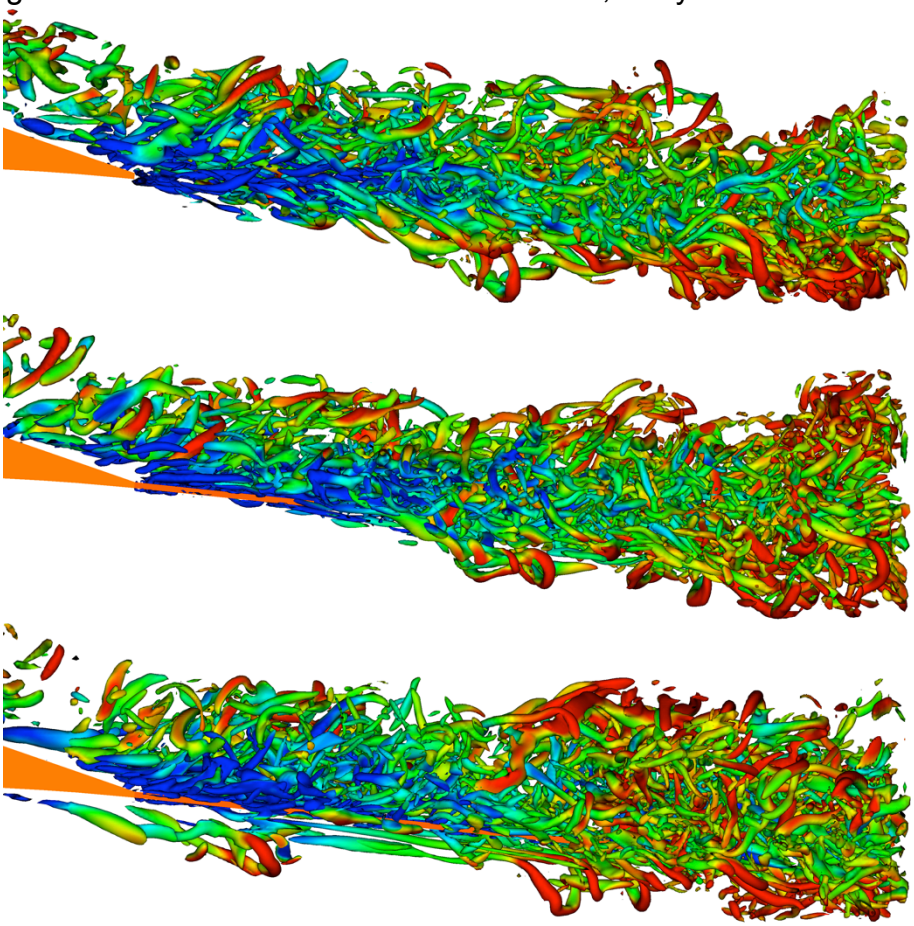

Figure 6: λ_2 (-2500) iso-surface plot colored with velocity magnitude (20-40 ms^{-1}): (top) clean case (middle) 5 % serrated case (bottom) 15 % serrated case

The mean and rms streamwise and wall normal velocity of the wake for the different trailing edges is given in Fig. 7 and 8 respectively. Clearly from both mean plots, the maximum velocity deficit is reduced and the wake seems to be the thickened as mixing is enhanced by the serrations. Near wake turbulence intensity in streamwise and wall normal direction on the other hand is increased, especially near the 15 % serrations. This is another indication for a thicker profile for the serrated trailing edges, due to enhanced mixing in this direction.

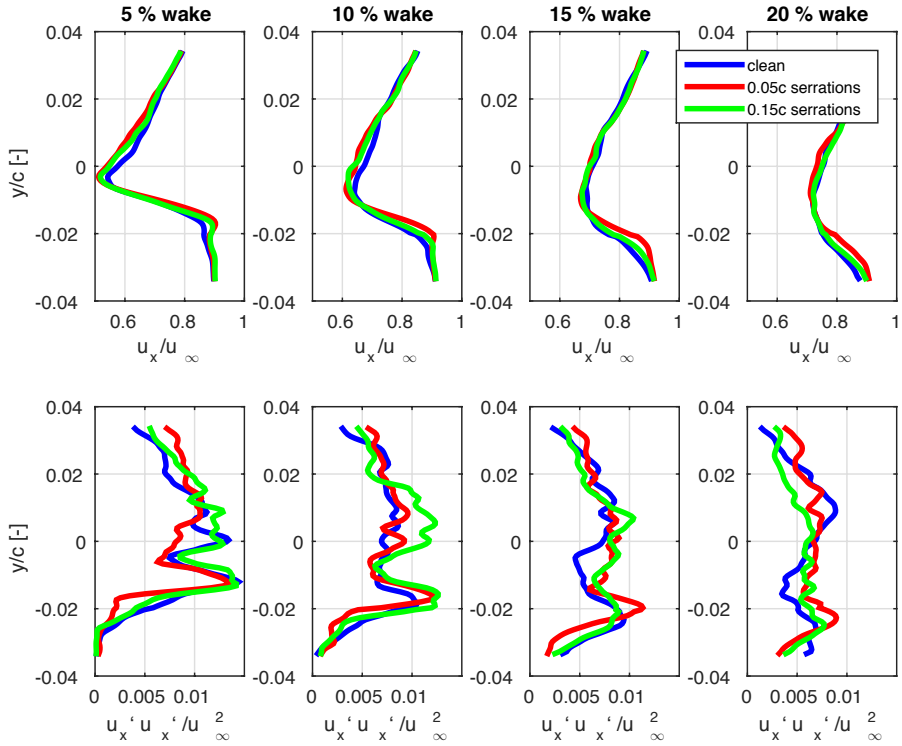

Figure 7: Mean streamwise velocity and fluctuations in the wake

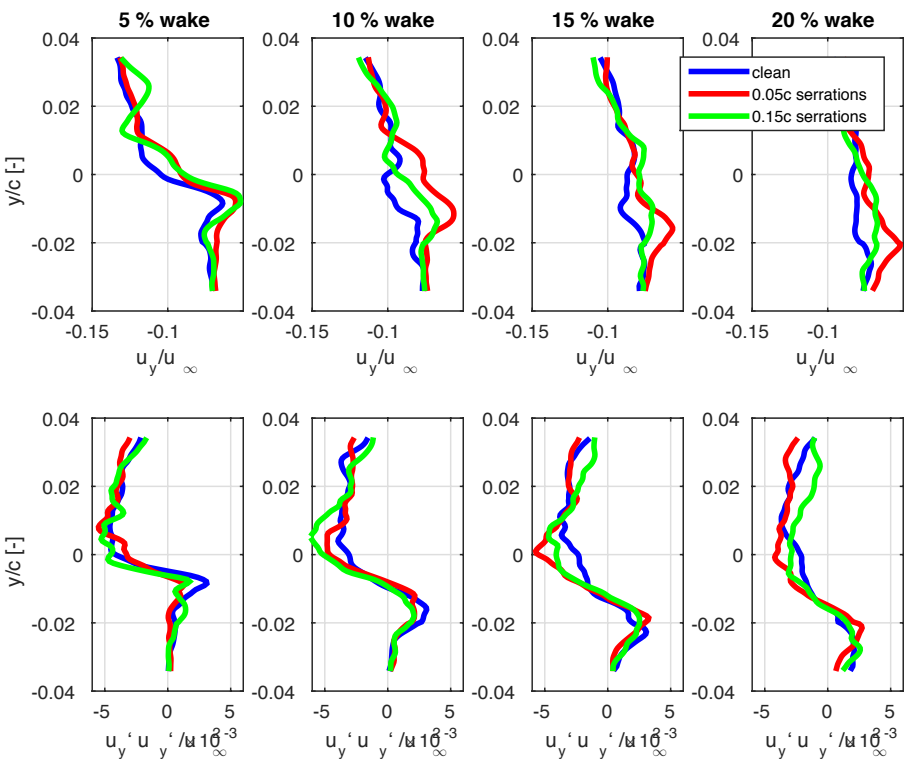

Figure 8: Mean wall-normal velocity and fluctuations in the wake

As mentioned, the spanwise coherence is a key parameter for determining the effectiveness of acoustic radiation of the turbulent eddies diffracted over the trailing edge. Therefore, the spanwise suction side coherence at 99 % of the chord is determined and plotted for each model in Fig. 9 by means of a contour plot for each single frequency. Many larger coherent structures (low frequencies) appear to be present at serrated edges, whereas smaller structures (mid frequencies) are more pronounced in the clean model. This is due to the gap between the serrations, where the pressure side boundary flow is sucked through and larger vortical structures become present and the wake is thickened. Overall, the coherence length, depicted in Fig. 10, illustrates that the decay is in line with the empirical reference line (Corcos 1964).

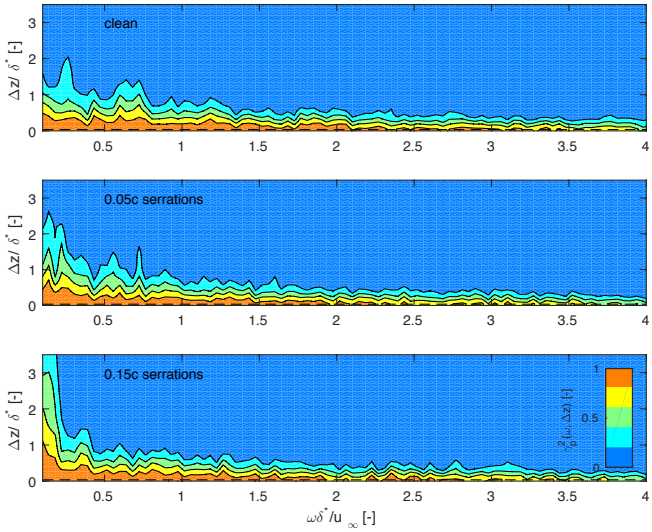

Figure 9: Contour plot of the coherence function

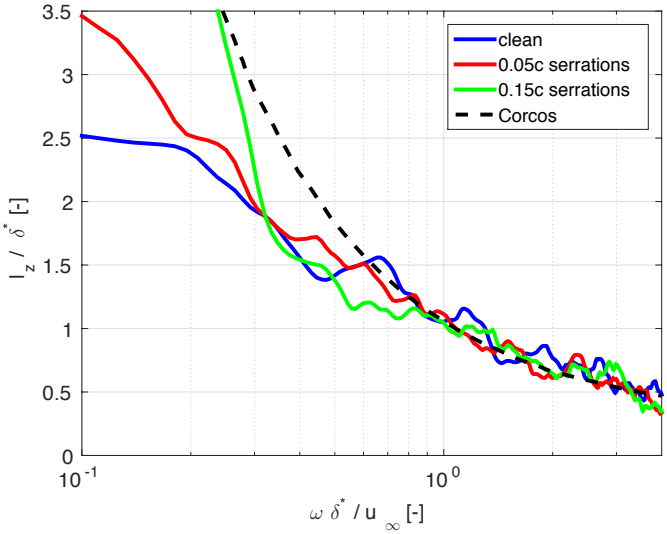

Figure 10: Coherence length plot

5. Acoustic results

The noise produced by the airfoil, the so-called airfoil self-noise is determined using the methodology prescribed in section 2.3. Wall pressure data is obtained from the flow simulation and used as source in the Ffowcs Williams and Hawkings analogy. The far field noise is recorded by 73 virtual microphones, all at a distance of two times the chord around the airfoil trailing edge. The Sound Pressure Level (SPL) of the probe directly above the trailing edge is given in Fig. 11, together with reference data from earlier mentioned studies. The slope, as well as the value of the line is in line with the experimental results of NREL (Devenport et al. 2008). A noise reduction due to the serrated edges is observed for St = 0.2 – 0.6 and for St = 0.6 – 2, corresponding to physical frequencies of approximately f = 250 – 750 Hz and 750 – 3000 Hz respectively. A maximum noise reduction of 5 dBA is achieved by either of the serrated edges. Further studies must be conducted to detect differences between various serrated edges, since currently, no clear conclusions can be drawn.

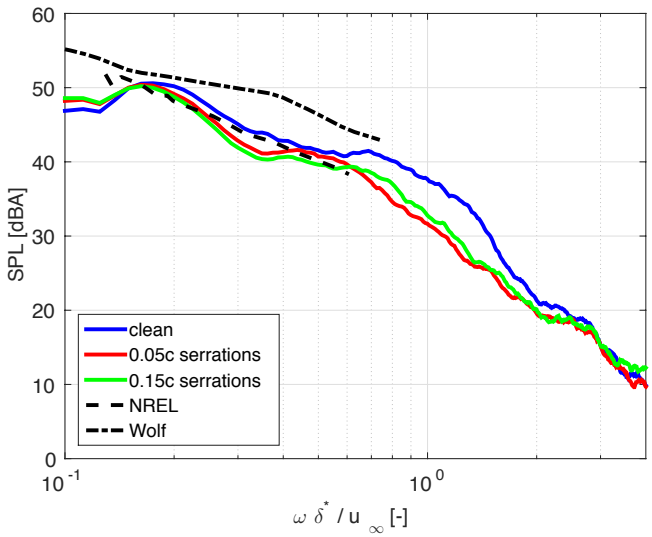

Figure 11: A-weighted Sound Pressure Level (SPL) at a distance of 2c above the trailing edge

In is interesting to further look at the noise reduction in terms of directivity effects by making use of Fig. 12. Clearly, the overall spectrum shows a single lobe in the direction of the leading edge, indicating the non-compactness of the acoustic source in such a way that the turbulent trailing edge noise is radiated in upstream direction. When specifically looking at the frequency range where the noise suppression add-on was most effective, the lobe is reshaped and

multiple lobes are formed. The serrated cases show a significantly drop in acoustic pressure level.

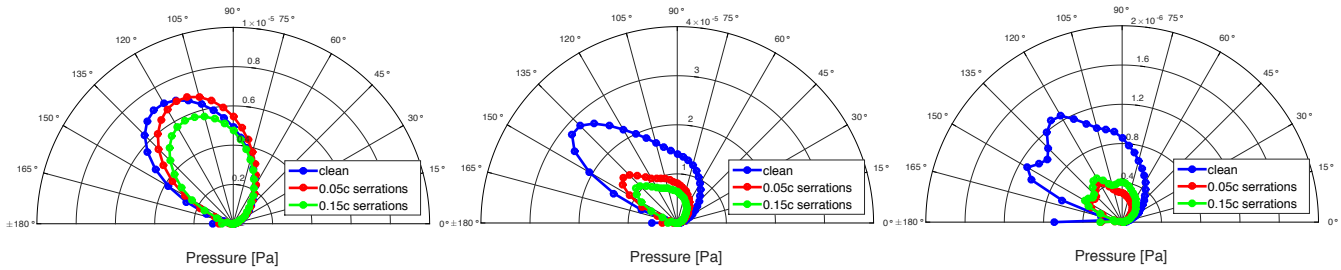

Figure 12: Directivity plot: (left) 250-10,000 Hz (middle) 400-1,000 Hz (right) 1,000-5,000 Hz

6. Conclusions

The use of the Lattice Boltzmann Method for fluid flow as well as the acoustic directivity around a clean and serrated DU96 wind turbine profile is investigated. Mean fluid flow parameters matches experimental and other previous studies. Turbulent structures and transition can be determined by the Lattice Boltzmann scheme and, in this study, are visualized by low-speed streaks and vortical structures by means of hairpin packets, full hairpins, legs and cane vortices. The serrated edges manipulate the flow in such a way, that the wake is thickened and turbulent structures are destructed. This phenomenon, which needs further attention in next studies, reduces the high frequency noise in the far field effectively up to 5 dBA. Non-compact behavior is observed by turbulent trailing edge noise convecting towards the leading edge in accordance with expectations. Further studies will focus on the inclusion of mesh resolution studies and relatively comparisons between different trailing edge add-ons.

References

Bhatnagar, P Gross, E and Krook, M (1954) *A model for collsion processes in gases. Small amplitude processes in charged and neutral one-component systems* Physical Review 94(3), 511-525

Blake, W (1986) *Mechanics of flow-induced sound and vibration, volumes I and II* Academic Press

Brès, G Pérot, F and Freed, D (2010) *A Ffowcs Williams-Hawkings Solver for Lattice-Boltzmann Based Computational Aeroacoustics*, 16th AIAA/CEAS Aeroacoustics Conference, AIAA-2010-3711

Brooks, T Pope, D and Marcolini, M (1989) *Airfoil self-noise and prediction* NASA Reference Publication 1218

Chen, S and Doolen G (1998) *Lattice Boltzmann method for fluid flows* Annual Review of Fluid Mechanics 30, 329-364

Chen, H (2003) *Extended Boltzmann kinetic equation for turbulent flows* Science 301(5633), 633-636

Christophe, J (2011) *Application of hybrid methods to high frequency aeroacoustics* University Libre de Bruxelles

Corcos, G (1964) *The structure of the turbulent pressure field in boundary layer flows* Journal of Fluid Mechanics 18(3), 353-378

Crouse, B Freed, D Senthooran, M Ullrich, S and Fertl S (2007) *Analysis of underbody windnoise sources on a production vehicle using the Lattice Boltzmann scheme* SAE Technical Paper 1(2400)

Devenport, W Burdisso, R Camargo, H Crede, E Remillieux, M Rasnick, M and van Seeters, P (2008) *Aeroacoustic testing of wind turbine airfoils* NREL Report, National Renewable Energy Laboratory

Drela, M (1989) *XFOIL: An analysis and design system for low Reynolds number airfoils* Low Reynolds Number Aerodynamics, University of Notre Dame Press, 1-12

Howe, M (1999) *Trailing edge noise at low Mach numbers* Journal of Sound and Vibration 225(2), 211-238

Oerlemans, S, Sijtsma, P and Mendez Lopez B (2007) *Location and quantification of noise sources on a wind turbine* Journal of Sound and Vibration 299(4-5), 869-883
Oerlemans, S Fisher, M Maeder ,T and Kögler K (2009) *Reduction of wind turbine noise using optimized aerofoils and trailing edge serrations* AIAA Journal 47(6), 1470-1481
Oerlemans, S and Fuglsang, P (2012) *Low-noise wind turbine design* EWEA Workshop Oxford
Palumbo, D (2012) *Determining correlation and coherence lengths in turbulent boundary layer flight data* Journal of Sound and Vibration 331(16), 3721-3737
Succi, S (2001) *The Lattice Boltzmann equation for fluid dynamics and beyond* Oxford University Press
Wolf, W Lele, S Jothiprasad, G and Cheung, L (2012) *Investigation of noise generated by a DU96 airfoil* 18th AIAA/CEAS Aeroacoustic Conference, AIAA 2012-2055